

Cavezzo, the first Italian meteorite recovered by the PRISMA fireball network. Orbit, trajectory, and strewn-field

D. Gardiol^{1*}, D. Barghini^{1,2}, A. Buzzoni³, A. Carbognani³, M. Di Carlo⁴, M. Di Martino¹, C. Knapic⁵, E. Londero⁵, G. Pratesi^{6,7}, S. Rasetti¹, W. Riva⁸, R. Salerno⁹, G. M. Stirpe³, G. B. Valsecchi^{7,10}, C. A. Volpicelli¹, S. Zorba⁵, F. Colas^{11,12}, B. Zanda^{13,11,12}, S. Bouley^{14,11,12}, S. Jeanne^{11,12}, A. Malgoyre^{15,12}, M. Birlan^{11,12}, C. Blanpain^{15,12}, J. Gattacceca^{16,12}, J. Lecubin^{15,12}, C. Marmo¹⁴, J.L. Rault^{17,11,12}, J. Vaubaillon^{11,12}, P. Vernazza^{18,12}, F. Affaticati¹⁹, M. Albani¹⁹, A. Andreis²⁰, G. Ascione²¹, T. Avoscan²², P. Bacci²³, R. Baldini²⁴, A. Balestrero⁸, S. Basso²⁵, R. Bellitto²⁶, M. Belluso²⁷, C. Benna¹, F. Bernardi²⁸, M. E. Bertaina², L. Betti²⁹, R. Bonino², K. Boros³⁰, A. Bussi²², E. Cascone³¹, C. Cattaneo³², A. Cellino¹, E. Colombi³³, M. Costa⁸, G. Cremonese³⁴, D. Cricchio³⁵, G. D’Agostino³⁶, M. D’Elia³⁷, P. De Maria²⁰, A. Di Dato³¹, R. Di Luca³, F. Federici³⁸, V. Gagliarducci³⁹, A. Gerardi³⁹, G. Giuli⁴⁰, D. Guidetti³, G. Interrante⁴¹, M. Lazzarin⁴², S. Lera³⁰, G. Leto²⁷, D. Licchelli⁴³, F. Manca⁴⁴, S. Mancuso¹, F. Mannucci⁴⁵, S. Meucci⁴⁶, A. Misiano³⁶, V. Moggi Cecchi⁶, E. Molinari⁴⁷, J. Monari⁴⁸, M. Montemaggi²⁶, M. Montesarchio⁴⁹, G. Monti⁵⁰, A. Nastasi³⁵, E. Pace⁵¹, R. Pardini³³, M. Pavone⁵², A. Pegoraro⁵³, S. Pietronave⁵⁰, T. Pisanu⁴⁷, N. Pugno⁵⁴, U. Repetti²², M. Rigoni³², N. Rizzi⁵⁵, C. Romeni³⁸, M. Romeo³⁶, P. Russo²¹, F. Salvati¹, D. Selvestrel³⁴, R. Serra⁵⁶, R. Smareglia⁵, M. Soldi³², R. Stanga²⁹, F. Strafella³⁷, C. Taricco², M. Tombelli⁴¹, P. Trivero⁵⁷, G. Umbriaco⁴², R. Vairetti⁵⁸, G. Valente⁵⁹, P. Volpini⁴⁶, R. Zagarella⁶⁰ and A. Zollo⁴⁹

Affiliations are listed at the end of the paper

Accepted XXX. Received YYY; in original form ZZZ

ABSTRACT

Two meteorite pieces have been recovered in Italy, near the town of Cavezzo (Modena), on January, 4th 2020. The associated fireball was observed on the evening of New Year’s Day 2020 by eight all-sky cameras of the PRISMA network, a partner of FRIPON. The computed trajectory sported an inclination angle of about 68° and a velocity at infinity of 12.8 km s⁻¹. Together with the relatively low terminal height, estimated in 21.5 km, those values were indicating the concrete possibility of a meteorite dropping event, as confirmed by the non zero residual total mass. The strewn-field was computed taking into account the presence of two bright light flashes, revealing that the meteoroid had been very likely subject to fragmentation. Three days after the event, two samples, weighing 3.6 g and 51.7 g, were collected as a result of a dedicated field search and thanks to the involvement of the local people. The two pieces were immediately recognised as freshly fallen fragments of meteorite. The computed proper elements, compared with the ones of known Near-Earth Asteroids from the NEODYs database, are compatible with one asteroid only, namely 2013 VC₁₀. The estimated original mass of the meteoroid, 3.5 kg, and its related size, about 13 cm, is so far the smallest among the currently 35 cases in which meteorites were recovered from precise strewn-field computation thanks to observational data. This result shows the effectiveness of accurate processing of fireball network data even on challenging events generated by small size meteoroids.

Key words: meteorites, meteors, meteoroids – methods: data analysis – techniques: image processing

* E-mail: danielle.gardiol@inaf.it

1 INTRODUCTION

The analysis of meteoritic material plays a relevant role in modern planetary sciences, since meteorites provide the easiest way to gather extra-terrestrial samples. The mineralogy and petrology of these samples is the major source of information about the geology, formation and evolution of minor and major bodies in the Solar System, and beyond (e.g. [Kruijer et al. 2020](#) and references therein). The scientific importance of such material is even higher if the interaction of the body with the Earth's atmosphere, generating the meteorite falls, is observed. In the first place, the observation of the meteor can provide crucial information about the physical properties of the body entering the atmosphere, which usually ablates for the most part before reaching the ground, if anything survives. In this case, the knowledge of the orbit of the meteoroid immediately prior to the impact unveils its origin in the Solar System, to be possibly linked with the physical and chemical characterisation of the meteorite itself. At the time of writing, the Meteoritical Database¹ lists almost 64000 officially classified meteorites. Among them, to the authors' knowledge only 35 (plus at least 2 not yet published) were collected together with a sufficient set of observations of their atmospheric path, allowing a reliable reconstruction of their heliocentric orbit before the interaction with the Earth's atmosphere. Gathering a sufficient statistics for meteoroid orbits would allow to infer about the link between meteorite types and their origin in the Solar System. Ultimately, the knowledge of the source regions of particular meteorite groups can provide constraints for the identification of a common parent body. As an example of recent relevant results on this topic, the reader can refer to [Granvik & Brown \(2018\)](#); [Jenniskens et al. \(2019\)](#); [Unsalan et al. \(2019\)](#). The importance of such results for planetary science is so pronounced that efforts have been made even to reconstruct meteorite pre-impact orbits from historical records ([Gounelle et al. 2006](#)).

The case of the Pribram meteorite in 1959 ([Ceplecha 1961](#)) represents the first successful meteorite recovery resulting from the observation of a bright meteor, which allowed for precise computations of its atmospheric trajectory, dynamics and dark flight. At the same time, this was the first meteorite recovery carried out thanks to a systematic meteors observation survey. Following the example of the Czechoslovakian Fireball Network, now European Fireball Network ([Spurný et al. 2017b](#)), many dedicated projects started to realise observational networks, both by amateur and professional astronomers, aiming to continuously monitor the night-sky and detect meteor and fireball events. The scientific outcome for this kind of survey is twofold, providing a unique tool to discover new meteor showers, by focusing on the faint but predominant component of the detected events, and capturing the very rare occurrence of meteorite-dropping fireballs. In this context, one should highlight that only 20 among the 35 'pedigree' meteorites were collected as a results of dedicated observational surveys (see Tab. 1). Excluding the well-known but out-of-range events of Almahata Sitta and Chelyabinsk, the remaining 13 falls were documented only through sporadic observations, like security cameras, dash cams and visual reports. For this reason, the past few years have witnessed a remarkable and still increasing effort to extend the coverage of meteor networks worldwide and maximise the efficiency in the recovery of meteorites. As a result, 9 among the 20 meteorites collected thanks to meteor surveillance networks were recovered only between 2014 – 2020.

In this international scenario, the PRISMA all-sky camera network ([Gardiol et al. 2016, 2019](#)) was born in 2016 to achieve a

systematic surveillance of meteors and fireballs in the skies over the Italian territory. In fact, PRISMA stands for 'Prima Rete Italiana per la Sorveglianza sistematica di Meteore e Atmosfera' (First Italian Network for Meteors and Atmosphere systematic Surveillance). At the time of writing, PRISMA has deployed 52 stations, among which 37 are fully operating and 15 are in installation phase. The PRISMA project is part of the international collaboration initiated by the FRIPON project (Fireball Recovery and InterPlanetary Observation Network, [Colas et al. 2014, 2015](#)).

In this paper we report on the finding of two meteorite pieces in Italy, near Cavezzo (Modena, Emilia-Romagna). The meteorite-dropping fireball, which reached a minimum absolute magnitude of -9.5, was observed on the evening of New Year's Day 2020 by eight all-sky cameras of the PRISMA network. The two fragments, weighing 3.6 g and 51.7 g respectively, were collected as a result of a dedicated field search and thanks to the involvement of the local people. In Sect. 2 we illustrate the preliminary strewn-field computation and the meteorite search activity, and give a short description of the two recovered fragments. Section 3 gives a complete review of the fireball data analysis and its physical characterisation. In Sect. 4 we provide the orbital parameters and discuss a possible progenitor for the observed meteoroid. We draw our conclusions in Sect. 5.

2 THE FIREBALL EVENT

2.1 Preliminary trajectory and strewn-field

On January 1st at 18:26:53 UT eight stations of the PRISMA network detected a brilliant fireball, namely IT20200101, in the skies of northern Italy (the list is shown in Tab. 2). The result of the alert system was computed over 4 cameras (ITPI03, ITTO02, ITER04, ITVE02) while the other ones were not completely configured in the automatic pipeline, having being installed since a short time. These preliminary results indicated the high probability of a meteorite-dropping bolide, as the pre-atmospheric velocity was about 12 km s⁻¹ and the inclination of the trajectory was high (68°). The light of the meteor was visible down to a height of about 22 km, and the lightcurve showed two sudden brightenings at altitude of about 32 and 30 km. In order to get a preliminary estimate of the strewn-field we reprocessed the data manually, adding two of the missing cameras (ITLO03 and ITER01). In the meantime we also started to receive dozens of reports from visual observers (52 observations reported through the PRISMA website on the International Meteor Organization online form²).

The high angle of fall resulted in an intense ablation process that led the fireball to shine with a mean absolute visual magnitude of about -7.5. The fireball disappeared from the camera images at an altitude of about 21.5 km. According to the first computation of the strewn-field, made using a purely ablative model, we estimated a nominal impact point laying around the village of Disvetro in the municipality of Cavezzo (province of Modena), near the local astronomical observatory, in the middle of the Po Valley. However, the lightcurve profile suggests that the object underwent a fragmentation process during the atmospheric flight, also confirmed by eyewitnesses. Therefore, we expected meteorite pieces to be spread around the line joining Disvetro with the on-ground projection of the final part of the visible trajectory, near the village of Rovereto sulla Secchia.

² https://prisma.imo.net/members/imo_view/event/2020/18

¹ The Meteoritical Society, <https://www.lpi.usra.edu/meteor/>

Table 1. List and relevant data of ‘pedigree’ meteorites, i.e., for which recovery was accompanied by a sufficient set of observations (optical, radio, infrasound, seismic, satellite), both sporadic or systematic, allowing for pre-impact orbit reconstruction. From left to right: name of the meteorite (approved by The Meteoritical Society), date of fall, preatmospheric velocity and mass, estimated terminal mass, meteorite total known weight (TKW) recovered on ground, minimum absolute magnitude recorded, impact energy (equivalent tons of TNT, $1 \text{ T} = 4.187 \cdot 10^9 \text{ J}$), fireball network which provided the observations (if any) and references for table data. The uncertainties associated to values of the table are not given here for simplicity, but can be found in respective references.

Name	Date UT	v_{∞} [km s ⁻¹]	m_{∞} [kg]	m_{fin} [kg]	TKW [kg]	M^{a}	E [T] ^b	Fireball Network ^c	Ref.
Příbram	07/04/1959	20.9	1300	80	5.6	-19	70	CFN	1,2
Lost City	04/01/1970	14.1	165	25	17	-12	4	PFN	3,4,5
Innisfree	06/02/1977	14.7	42	4.9	4.58	-12.1	1	MORP	5,6
Benešov	07/05/1991	21.3	4100	300 ^d	0.0116	-19.5	200	EFN	5,7,8,9
Peekskill	09/10/1992	14.7	5000	-	12.4	-16	130	-	2,10
Tagish Lake	18/01/2000	15.8	56000	1300	10	-22	1700	-	11,12,13
Morávka	06/05/2000	22.5	1500	100	1.4	-20	90	-	14,15,2
Neuschwanstein	06/04/2002	20.9	300	20	6.22	-17.2	16	EFN	16,17,18
Park Forest	27/03/2003	19.5	11000	-	30	-21.7	500	-	19,20
Villalbeto de la Peña	04/01/2004	16.9	600	13	5.2	-18	20	-	21,22,23
Bunburra Rockhole	20/07/2007	13.4	22	1.1	0.339	-9.6	0.5	DFN	24,25
Almahata Sitta	07/10/2008	12.4	40000	39	10.7	-19.7	730	-	26,27,28,29
Buzzard Coulee	21/11/2008	18.0	10000	-	>200	-20	390	-	30,31,32
Maribo	17/01/2009	28.3	2000	<20	0.0258	-20	190	-	33,34
Jesenice	09/04/2009	13.8	170	20	3.611	-15	4	SFN	35,36
Grimsby	26/09/2009	20.9	30	5	0.215	-14.8	2	SOMN	37
Košice	28/02/2010	15.0	3500	500	11.3	-18	100	-	38,39
Mason Gully	13/04/2010	14.5	40	-	0.0245	-9.4	1	DFN	40,41
Křiževci	04/02/2011	18.2	50	<5 ^e	0.291	-13.7	2	CMN	42
Sutter’s Mill	22/04/2012	28.6	40000	-	0.943	-19	4000	-	43
Novato	18/10/2012	13.7	80	-	0.363	-13.8	3	CAMS	44
Chelyabinsk	15/02/2013	19.0	$1.2 \cdot 10^7$	10000	730	-27.3	$5 \cdot 10^5$	-	45,46,47
Annama	18/04/2014	24.2	470	12.5	0.1679	-18.3	30	FFN	48,49,50
Žďár nad Sázavou	09/12/2014	21.9	150	>1.3 ^f	0.087	-15.3	9	EFN	51
Porangaba	09/01/2015	-	-	-	0.970	-	-	-	52
Saričiček	02/09/2015	17.3	1700	-	24.78	-16.8	60	-	53
Creston	23/10/2015	16.0	50	-	0.8523	-12	2	CAMS, SACN	54
Murrili	27/11/2015	13.7	38	2	1.68	-	0.9	DFN	55,56
Ejby	06/02/2016	14.5	120	-	8.982	-14.0	3	-	57,58
Stubenberg	06/03/2016	14	600	-	1.473	-15.5	14	EFN	59,60
Hradec Králové	17/05/2016	-	-	-	0.134	-11.5	-	EFN	61,62
Dishchii’bikoh	02/06/2016	16.6	1000 ^g	-	0.07957	-16	30	CAMS, SACN	63,64
Dingle Dell	31/10/2016	15.4	40	1.4	1.150	-	1	DFN	65
Hamburg	17/01/2018	15.8	140	>1	~1	-16.3	5.5	-	66,67
Renchen	10/07/2018	20	50 ^h	-	1.227	-13.4	2	EFN	61,68
Cavezzo ⁱ	01/01/2020	12.8	3.5	1.5	0.0553	-9.5	0.07	PRISMA	This work

^a Magnitude values are given in different passbands (e.g. visual, panchromatic) and might be not strictly comparable one another ^b The impact energy was computed by the author, if not provided in the original work, or updated to more precise estimates of preatmospheric mass and/or velocity ^c CFN = Czechoslovakian Fireball Network (now EFN), PFN = Prairie Fireball Network, MORP = Meteorite Observation and Recovery Project, EFN = European Fireball Network, DFN = Desert Fireball Network, SFN = Slovakian Fireball Network (part of EFN), SOMN = Southern Ontario Meteor Network, CMN = Croatian Meteor Network (part of EFN), CAMS = Cameras for All-sky Meteor Surveillance, FFN = Finnish Fireball Network, SACN = Spalding Allsky Camera Network, SkySentinel ^d Most of the terminal mass in gram-sized meteorites ^e Apart from the main mass, just a few 10 – 100 g meteorites are expected and ~ 2000 meteorites with mass > 1 g ^f Main mass of 1.3 kg plus a second largest meteorite in the range 100 – 200 g (~ 250 meteorites in the range 10 – 200 g, 6 kg total, and ~ 3000 meteorites of 0 – 1 g, 7 kg total) ^g There is a disagreement between meteoroid size deduced from radiated energy from satellite observations (~ 15000 kg) and cosmogenic radionuclide data (400 – 1800 kg) ^h Computed by the author considering a preatmospheric radius of 10 – 20 cm deduced from cosmogenic ²⁶Al data and a bulk density of 3.4 g cm⁻³ (reference 68), assuming a spherical shape. ⁱ Meteorite name not yet approved by the Meteoritical Society. At time of writing, a classification proposal had been submitted to Nom. Com. of the Meteoritical Society. References: [1] Ceplecha (1961) [2] Borovička & Kalenda (2003) [3] McCrosky et al. (1971) [4] Ceplecha (1996) [5] Ceplecha & Revelle (2005) [6] Halliday et al. (1981) [7] Spurný (1994) [8] Borovička et al. (1998) [9] Spurný et al. (2014) [10] Brown et al. (1994) [11] Brown et al. (2000) [12] Brown et al. (2002) [13] Hildebrand et al. (2006) [14] Borovička et al. (2003a) [15] Borovička et al. (2003b) [16] Spurný et al. (2002) [17] Spurný et al. (2003) [18] Revelle et al. (2004) [19] Simon et al. (2004) [20] Brown et al. (2004) [21] Llorca et al. (2005) [22] Trigo-Rodríguez et al. (2006) [23] Bischoff et al. (2013) [24] Bland et al. (2009) [25] Spurný et al. (2012) [26] Jenniskens et al. (2009) [27] Borovička & Charvát (2009) [28] Shaddad et al. (2010) [29] Welten et al. (2010) [30] Hildebrand et al. (2009) [31] Milley et al. (2010) [32] Wilson & McCausland (2012) [33] Haack et al. (2012) [34] Borovička et al. (2019) [35] Spurný et al. (2010) [36] Bischoff et al. (2011) [37] Brown et al. (2011) [38] Borovička et al. (2013a) [39] Tóth et al. (2015) [40] Spurný et al. (2011) [41] Dyl et al. (2016) [42] Borovička et al. (2015) [43] Jenniskens et al. (2012) [44] Jenniskens et al. (2014) [45] Popova et al. (2013) [46] Borovička et al. (2013b) [47] Brown et al. (2013) [48] Trigo-Rodríguez et al. (2015) [49] Kohout et al. (2017) [50] Bouvier et al. (2017) [51] Spurný et al. (2020) [52] Ferus et al. (2020) [53] Unsalan et al. (2019) [54] Jenniskens et al. (2019) [55] Bland et al. (2016) [56] Sansom et al. (2020) [57] Spurný et al. (2017a) [58] Haack et al. (2019) [59] Spurný et al. (2016) [60] Bischoff et al. (2017) [61] Spurný et al. (2019) [62] Gattacceca et al. (2019) [63] Palotai et al. (2019) [64] Jenniskens et al. (2020) [65] Devillepoix et al. (2018) [66] Brown et al. (2019) [67] Gattacceca et al. (2020) [68] Bischoff et al. (2019)

Table 2. PRISMA stations that observed IT20200101. From left to right: station name, latitude, longitude and elevation above sea level.

Station name	Lat. N [°]	Long. E [°]	El. [m]
Bedonia (ITER04)	44°30'27"7	09°37'57"0	550
Rovigo (ITVE02)	45°04'54"0	11°47'42"2	15
Felizzano (ITPI03)	44°54'45"0	08°26'14"0	114
Loiano (ITER01)	44°15'23"7	11°19'54"4	787
Cecima (ITLO03)	44°48'52"7	09°04'43"6	670
Navacchio (ITTO02)	43°40'59"5	10°29'29"9	15
Padova (ITVE01)	45°24'07"0	11°52'06"7	64
Asiago (ITVE03)	45°50'57"9	11°34'06"0	1370

2.2 Meteorite search and recovery

As soon as the preliminary strewn-field was identified (the day following the fall, i.e., January 2nd in the early afternoon) we had to decide a strategy for the meteorite search. Within the PRISMA collaboration a team of volunteers, both professionals and amateurs, is trained for meteorite hunting and dedicated to search activities. The strewn-field, between the towns of Rovereto sulla Secchia and Disvetto, lies in a rural territory with many cultivated fields, groves and houses spread over the area. The vast majority of the terrain is private property, so we alerted the local authorities that teams of hunters would be there to search for meteorites on behalf of the PRISMA collaboration. To help searchers enter private terrains and areas, we also involved the Civil Protection of Cavezzo, as they are usually employed during public events, and their members are well known among the population. At the same time we prepared a press release to be published on the PRISMA website³ and on the outreach platform of INAF (MediaINAF)⁴. In the press release we provided all the necessary information about the most probable area where fragments could be found and also a brief tutorial on how to recognise a freshly fallen meteorite. The goal of this strategy was to maximise the probability of a successful recovery by involving a larger number of people, although not specifically trained. The press release was sent also to local media in the Modena area encouraging local inhabitants to start their own search or at least to be aware that they may chance upon meteorite fragments, and in this case to contact us by email. The news was made public on late afternoon of January 2nd, and already on January 3rd we started receiving reports from people in the local area and giving interviews to local and national newspapers and televisions. By January 4th in the morning a team of some twenty hunters was ready to start searches on Sunday 5th, while a small scouting group from Bologna University led by Romano Serra was already on-site. On January 4th at 3 PM local time we received an email with the first reliable meteorite candidate from Mr. Davide Gaddi, reporting the recovery of a small fragment (the size of a fingernail) on an embankment along the Secchia river. We immediately arranged a meeting with Romano Serra, where Mr. Gaddi showed also a second larger fragment, found in the meantime in the same place, the size of a big walnut. Both fragments were recognised to be freshly fallen meteorites. It was less than three days from the fireball event.

In the following days the search for other fragments carried out by teams organised by PRISMA and by other people did not lead to fur-

³ <http://www.prisma.inaf.it/index.php/2020/01/02/una-meteorite-in-emilia-romagna>

⁴ <https://www.media.inaf.it/2020/01/02/forse-e-caduta-una-meteorite-in-emilia-romagna>

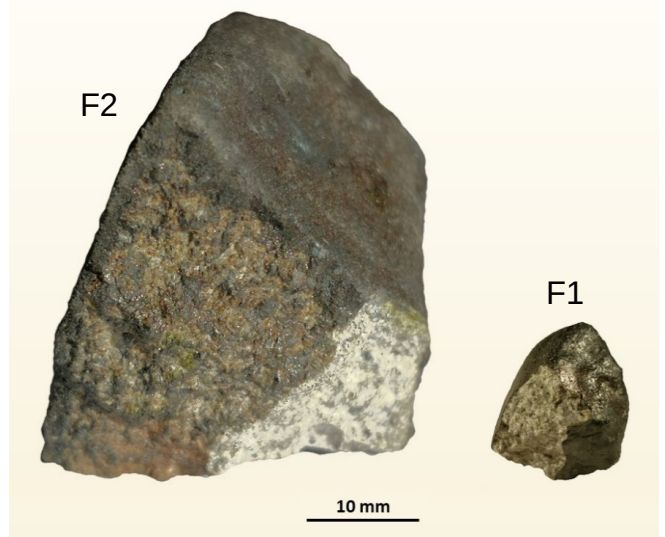


Figure 1. The two recovered samples of the Cavezzo meteorite. On the right, the first recovered fragment (F1, 3.6 g); on the left, the second and larger one (F2, 51.7 g).

ther findings, even though a refined strewn-field was in the meantime available. Bad weather and muddy fields also limited the area available for the quest. We planned to resume searches in Spring 2020 hoping for better weather and terrain conditions, but the COVID-19 pandemic break did not allow us to organise further on-field activities up to now.

2.3 Meteorite fragments description

The two fragments were recovered at coordinates 44°49'43"7 N 10°58'19"5 E, at the border of a narrow country road parallel to the left main embankment of the Secchia river, approximately halfway between Villa Motta and Rovereto sulla Secchia, in the territory of the Cavezzo municipality. Figure 1 shows the two finds. Fragment n.1 (F1), the first one to be found, has a tetrahedral form and weighs 3.6 grams. Fragment n.2 (F2), the largest one, weighs 51.7 grams. Both fragments clearly present a recently formed fusion crust on most of their surface, while showing a light grey apparently chondritic pattern on one of their sides due to fragmentation most likely occurred while hitting the ground. This interpretation is corroborated by the presence of an impact feature present on one of the edges separating two sides, accompanied by white streaks (Fig. 2a). F2 also presents a darker gray colouration on one side, apparently a less pronounced secondary fusion crust, compatible with exposure due to a fragmentation most probably associated to the brightening which occurred at the height of around 30 km.

The meteorite fragments are currently being analysed at the Department for Earth Science of the Firenze University for classification and to obtain mineralogical, petrographic and geochemical information. The result of this extensive analysis will be the subject of a dedicated article (Pratesi et al. 2020, submitted). However, all data point toward an L chondritic group, although the differences between the two fragments are so strong that an anomalous nature of the meteorite has been suggested in the proposal submitted to the Nomenclature Committee of the Meteoritical Society. Figure 2b shows a photomosaic of polarising optical microscope images of a thin sections obtained from F2, where chondrules and chondrule

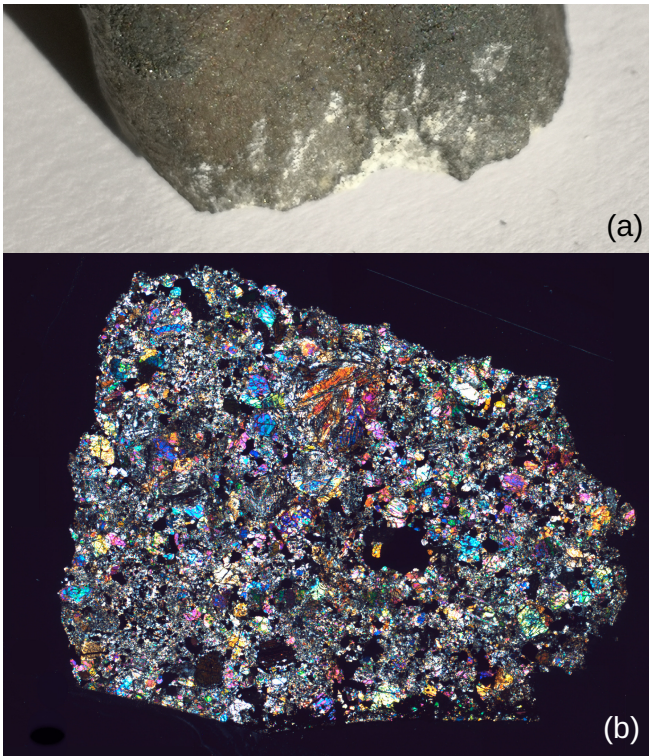


Figure 2. Details of the larger fragment F2 of the Cavezzo meteorite. (a) White streaks occur on one edge of F2, suggesting on-ground breakup of the original body; (b) photomosaic of polarising optical microscope images (transmitted light, crossed polars) of a thin sections obtained from F2 (field width 12 mm).

fragments distributed in the matrix can be observed.

The γ -ray activity measurement performed on F2 at Monte dei Cappuccini laboratory in Torino (Taricco et al. 2006; Colombetti et al. 2013) has shown the presence of many cosmogenic radioisotopes. Despite the small mass of F2 with respect to the samples commonly measured in this facility, the two characteristic lines of ^{48}V at 983.53 and 1312.11 keV⁵ are clearly visible, indubitably confirming the presence of this radioisotope. Since ^{48}V has a half-life of 15.97 d, this is an indisputable proof of the very recent fall of the recovered meteorite, thus linking it again to the New Year’s fireball. The results of the radiometric measures of F2 will be the subject of a forthcoming publication.

3 FIREBALL DATA ANALYSIS

PRISMA, as a partner of the FRIPON collaboration, currently shares the same technology of the network. Each station is equipped with a CCD camera (6 mm diagonal, 1296 x 966 px) coupled with a short focal lens objective (1.25 mm), to obtain a wide field of view (FOV) of approximately $223^\circ \times 166^\circ$. The camera is connected to a Linux operating mini-PC via LAN and controlled by the open-source FREETURE software (Audureau et al. 2014). The camera is operated at 30 fps (1/30 s exposure time) in order to sample the meteor trail with a suitable rate. The meteor detection

is triggered locally in each node by a frame difference method, and cross-correlated with respect to data of other nodes to check for multiple detections of the same event. The 30 fps video stream of the detected meteor is saved locally as FITS files and, in the case of a multiple detection, it is collected by the FRIPON central server, located at the Laboratoire d’Astrophysique de Marseille (LAM). PRISMA data are also synchronised and stored at the IA2 (Italian Center for Astronomical Archives) INAF archiving facilities in Trieste (Knapić et al. 2014). The PRISMA reduction pipeline is developed in IDL⁶ v8.7 and MATLAB⁷ Release 2015b.

The first step in the analysis of meteor detections is the astrometric and photometric reduction. Since almost no stars arise from the background noise in the 30 fps video stream, the control software acquires a 5 s exposure image, named *capture*, every 10 minutes. With a limiting V magnitude of about +4.5 on this set of images, available for each operational night, some hundreds of stars per frame are automatically identified, correlated with catalogue positions and therefore used as a reference for both astrometric and photometric calibration. Concerning astrometry, we implemented the approach introduced by Cepelcha (1987); Borovička (1990); Borovička et al. (1995), in which the absolute astrometric solution of the camera is derived, in the alt/az system, as a function of 8 parameters. This analytical description accounts for the major distortion factors that are, in the case of PRISMA all-sky cameras, the pronounced radial distortion of the fish-eye lens and the possible mismatch of the optical centre with respect to the local zenith direction. Two additional parameters are introduced if the optical plate results to be misaligned with respect to the local horizon plane. With respect to Borovička et al. (1995), we provided a new explicit parametrisation of the astrometric model, which reduces the parameters’ correlation degree and improves overall convergence properties for the determination of the astrometric solution (Barghini et al. 2019a). At the same time, the photometric calibration is determined on the same set of images as well. Since no filter is applied over the lens, a wide passband magnitude is considered, roughly between 400 and 800 nm, on the basis of the quantum efficiency of the camera and the transmission of the glass dome. This panchromatic magnitude is numerically computed from the catalogue *UBVRI* Johnson-Cousins system and therefore used to derive the zero-point and atmospheric extinction coefficient for each capture. For PRISMA cameras, we also determined and therefore accounted for the efficiency loss along the radial direction, that turns out to be of about 40 per cent from the centre to the very edge of the camera (Barghini et al. 2019b).

To estimate the fireball atmospheric trajectory and its main physical parameters and to compute the best kinematic parameters in the terminal point of the luminous path, we used the method outlined in Carbognani et al. (2020). The atmospheric trajectory computation is performed according to the classical formulation reported in Cepelcha (1987); Borovička (1990). The parameters of the dynamical model are derived based on the description given by Kalenichenko (2006) and references therein. In our case, however, the meteoroid has been most probably subject to important fragmentation phenomena, so that the physical quantities are to be taken with caution. For the dark flight and strewn-field determination again Cepelcha (1987) formulation is used, computing

⁶ IDL – Interactive Data Language – Harris Geospatial Solutions, Inc. – <https://www.harrisgeospatial.com/>

⁷ MATLAB – Matrix Laboratory – MathWorks, Inc., – <http://www.mathworks.com>

⁵ NUDAT database – <https://www.nndc.bnl.gov/nudat2/>

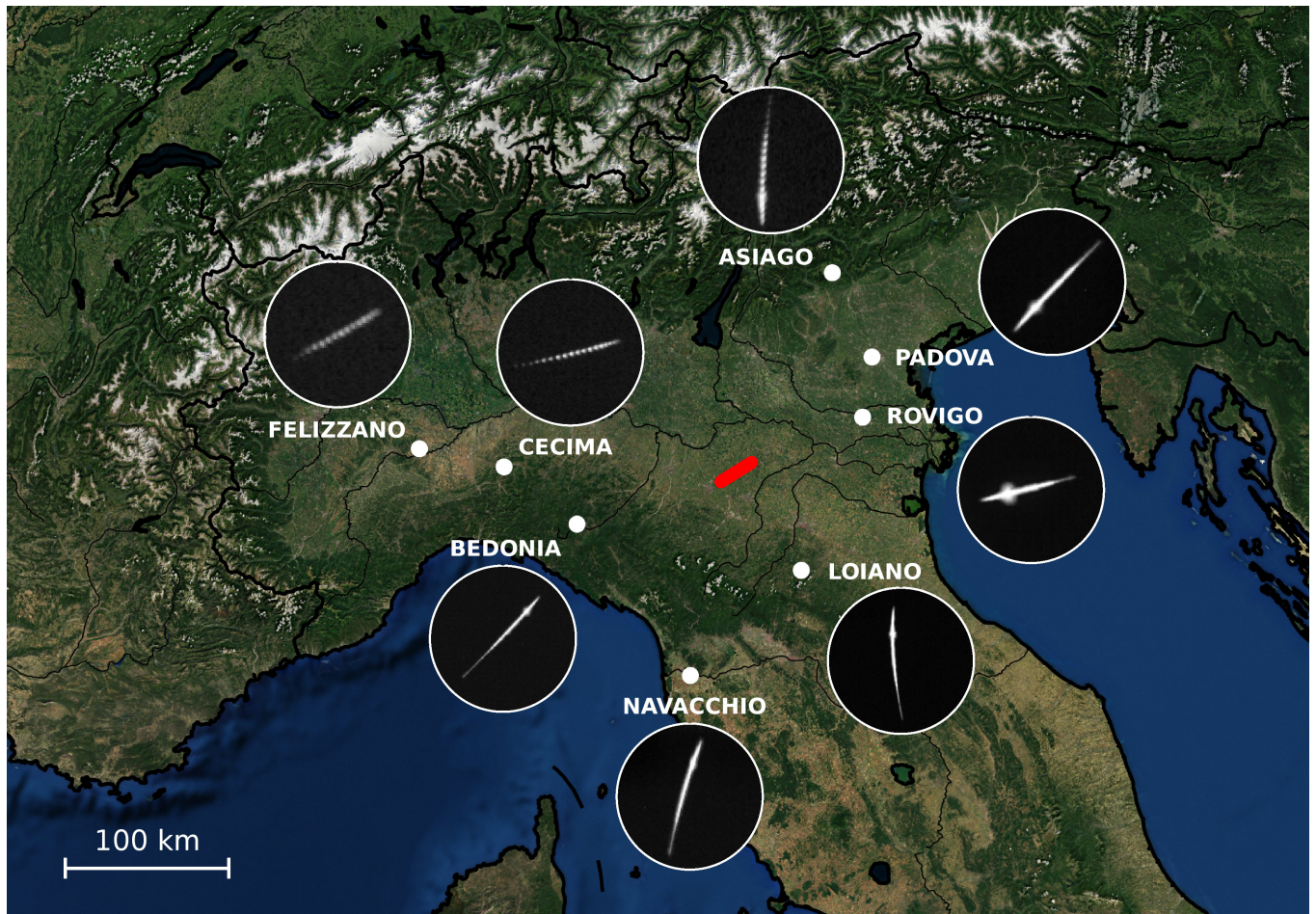


Figure 3. Map of the PRISMA stations (white dots) involved in the detection of the IT20200101 fireball. The red line plots the fireball bright trajectory projected on ground, and white circles enclose the fireball trail seen by each camera (reconstructed from video records). Please notice that fireball trails are oriented accordingly to the specific in-situ hardware installation, and may be not strictly consistent with one another (all-sky images, from which meteor trails are cropped, were approximately oriented with N direction upward and E direction leftward). Background map was generated using the Matplotlib Basemap Toolkit ([Hunter 2007, https://matplotlib.org/basemap/users/index.html](https://matplotlib.org/basemap/users/index.html))

the expected impact points in a range of mass-section ratios. The orbital parameters are derived both in an analytical way (Ceplecha 1987) and by numerical integration, as the two methods have proven to provide consistent results (Clark & Wiegert 2011).

3.1 Astrometry and photometry

Figure 3 shows the map of PRISMA stations which detected the IT20200101 fireball (white dots) together with the on-ground projection of the reconstructed trajectory (red line) and the images of the meteor trail seen by each camera (enclosed in white circles), obtained through the analysis of video records. The distance between the eight stations and the fireball atmospheric trajectory spans between 75 and 200 km. While some cameras captured its bright flight in the central area of the FOV, other cameras recorded the fireball at a quite low elevation above the horizon. In particular, the astrometric reduction for data of two cameras (Felizzano and Cecima) results in elevations lower than 10° for the final 5-10 points of the trajectory. Unfortunately, sky quality condition is not optimal in many PRISMA observational sites, due to light pollution which is espe-

cially severe in the Po valley. These experimental constraints prevent us from detecting stars, even in long-exposure calibration images, below 10° of elevation for most PRISMA cameras. While residual systematic effects are numerically corrected in our astrometric reduction pipeline (Barghini et al. 2019b), this correction can be only tentative below 10° of elevation and the positional accuracy for these last points is questionable. To assess the potential effect of this bias over the final result of our pipeline, we first excluded these points and verified that the overall results (i.e., trajectory computation) were unchanged within measurement errors, with their total weights not being predominant over other reference points, at same timing, from the remaining six cameras. We finally included them since they provide important photometric data for the trailing edge of the fireball lightcurve.

The photometric analysis highlights that the fireball point spread function (PSF) saturated, in almost all cameras, between 2 and 4.7 s from the beginning of the bright flight. Barghini et al. (2019b) give a comprehensive analysis of the effects of PSF saturation for PRISMA cameras, and concludes that astrometric precision is not significantly degraded at least below $h \leq 4$, being h the relative ratio of the PSF height to the saturation value, namely 4095 ADU (analogic-to-digital

Table 3. IT20200101 fireball parameters obtained from triangulation and dynamical model. The two columns refer to values at the beginning and end of the bright flight respectively (when applicable). Values of mass and diameter are computed from the mass-section ratio D (in the hypothesis of pure ablation) by assuming a spherical shape of the meteoroid and for the measured meteorite bulk density of 3.322 g cm^{-3} .

		Beginning	Terminal
Time (UT)	t	18:26:52.9	18:26:58.5
Height [km]	h	75.9 ± 0.2	21.5 ± 0.1
Latitude (N)	ϕ	$44^\circ 44' 03'' \pm 7''$	$44^\circ 50' 24'' \pm 7''$
Longitude (E)	λ	$10^\circ 43' 09'' \pm 7''$	$10^\circ 57' 25'' \pm 7''$
Velocity [km s^{-1}]	v	12.2 ± 0.2	4.0 ± 0.2
Mass-section ratio [kg m^{-2}]	D	280 ± 20	210 ± 20
Mass [kg]	m	3.5 ± 0.8	1.5 ± 0.4
Diameter [m]	d	0.13 ± 0.01	0.09 ± 0.01
Luminous path length [km]	L	59	
Duration [s]	T	5.6	
Trajectory inclination [$^\circ$]	T_i	68.4 ± 0.3	
Trajectory azimuth [$^\circ$]	az	238.1 ± 0.2	
Min. absolute magnitude	M	-9.5 ± 0.5 @ 32.6 km	
Pre-atmospheric velocity [km s^{-1}]	v_∞	12.8 ± 0.2	
Ablation coefficient [$\text{s}^2 \text{ km}^{-2}$]	σ	0.012 ± 0.003	
Max. dynamic pressure [MPa]	P_{max}	1.0 ± 0.3 @ 28.2 km	
Impact Energy [T TNT]	E	0.07 ± 0.02	

units) for PRISMA 12-bit video records. To account for count loss on the saturated portion of the PSF, a tentative correction is applied by fitting a bidimensional gaussian model to non-saturated pixels of the PSF. This analysis therefore aims to estimate the original PSF shape and unveils h values mostly below 2, and always below 4 also for the two bright flares (Sect. 3.2). These conclusions are also confirmed by a visual inspection of the saturated portion of the PSF, which is confined to few pixels in the very centre of it for the most part of the trajectory. From this approach, a saturation correction factor is therefore estimated and applied to results obtained through aperture photometry. The computed count loss fraction for the saturated fraction of the bright flight is mostly confined under 30 per cent and raises up to about 50 per cent in correspondence of the brightest flare.

3.2 Atmospheric trajectory and dynamical model

The results of the atmospheric trajectory and dynamical model computation are summarised in Tab. 3 and Fig. 4. In particular, Fig. 4a shows the height of the fireball above ground as a function of time since the beginning of the luminous path. The observed fireball trajectory begins at a starting height $h_b = 75.9 \pm 0.2 \text{ km}$ and exhausts at a terminal height $h_t = 21.5 \pm 0.1 \text{ km}$. The total length of the luminous atmospheric path is about 59 km, which was covered in about 5.6 s. The meteoroid followed an atmospheric trajectory inclined by an angle of about $68^\circ 4 \pm 0^\circ 3$ with respect to the horizontal plane, with an azimuth of about $238^\circ 1 \pm 0^\circ 2$, travelling from WSW to ENE and entered rapidly into the denser layers of the atmosphere. The height residuals of observed points with respect to the computed trajectory are plotted in Fig. 4b. The standard deviation of $\sigma_h = 0.25 \text{ km}$, considering the distance of the bolide to the observing stations, corresponds to angles less than $10'$ and therefore always below the pixel resolution of our cameras. Systematic patterns are visible along the trajectory. Above 50 km of altitude the descent of the body into the atmosphere is slower compared to the fitted trajectory. Furthermore, after the two flare events, an increased spreading of the height residuals is evident. Systematic effects associated to specific cameras may be related to PSF asymmetries that affects the most part of the

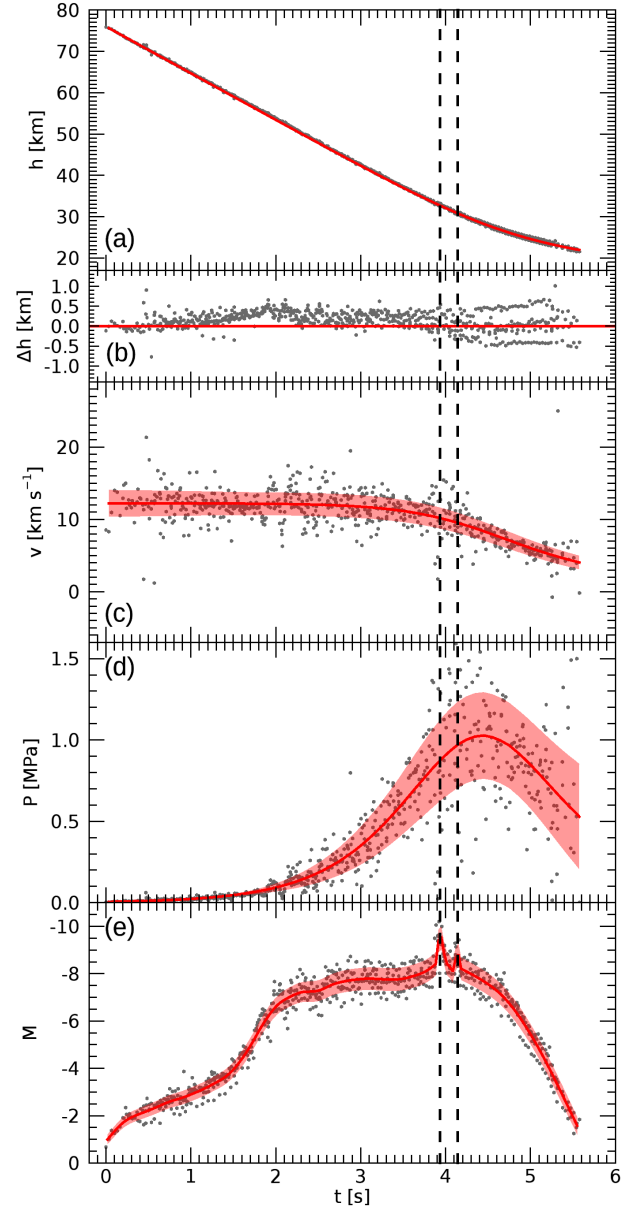


Figure 4. Results of trajectory computation and dynamic model for the IT20200101 fireball. (a) Vertical projection of the atmospheric trajectory; (b) vertical residuals of the atmospheric trajectory; (c) fireball velocity with respect to ground; (d) aerodynamic pressure (Eq. 1); (e) absolute magnitude (at 100 km, zenith of the observer). In every panel, grey points plot measured or computed values for the single stations, whereas the red line plots the nominal fit values (a-c) or a smoothed version of grey points (d,e). Red shaded areas enclose 1σ uncertainty.

trajectory.

The observed velocity (Fig. 4c) allowed us to derive an entering speed of $12.2 \pm 0.2 \text{ km s}^{-1}$ at 76 km of altitude, which started to decrease only in the denser layers of the atmosphere below 30 km, just after the brightenings where it lowered to 10 km s^{-1} . At the end of the luminous path, 21.5 km above ground, the meteoroid slowed down to $4.0 \pm 0.2 \text{ km s}^{-1}$.

The absolute magnitude light curve is shown in Fig. 4e. In the first two seconds the brightness grew rapidly, reaching a plateau of about

$M = -7.5$ between $t = 2.0$ and 4.7 s, followed by a sudden fading in the last second. Two rapid flares are visible at 3.95 s and 4.15 s with absolute magnitudes close to -9.5 and -8.5 respectively, related to the already mentioned fragmentation. The corresponding altitudes are about 32.6 and 30.7 km respectively, when the meteoroid was still moving at a speed of about 10.1 km s $^{-1}$. Usually the meteoroids fragmentation models assume that the fragmentation process starts when the aerodynamic pressure is equal to the mechanical strength S . According to the meteoroid height h and speed V in the main explosion Foschini (1999), we can estimate a strength of about:

$$S = \frac{\gamma - 1}{\gamma} \rho_{sl} V^2 e^{-h/H} \approx 0.88 \text{ MPa}, \quad (1)$$

where $\gamma \sim 1.7$ is the ratio of specific heats, $H \approx 8$ km is the atmospheric scale height and $\rho_{sl} \approx 1.22$ kg m $^{-3}$ is the atmospheric density at sea level. This value is close the maximum aerodynamic pressure that is attained at an height of about 28.2 km (see Fig. 4d). Since Cavezzo is a stony meteorite, a strength of about 10 MPa could be expected, one order of magnitude greater. However, it is common case to observe fragmentations at aerodynamic pressure well below 1 MPa and even down to few tens of kPa (for example, see Popova et al. 2011; Devillepoix et al. 2019). This evidence suggests a particular weakness of the meteoroid caused, for instance, by fractures already present when entering the atmosphere or porosity of the material.

Given the measured density of the recovered fragments of 3.322 g cm $^{-3}$ and by assuming a spherical shape for the entering meteoroid, the computed value for the mass-section ratio D derived by the dynamical model provides an estimate of the mass and size before and after the luminous atmospheric transit, in a purely ablative regime. The meteoroid pre-atmospheric mass can be estimated to be 3.5 ± 0.8 kg ($D = 280 \pm 20$ kg m $^{-2}$) with a diameter of 0.13 ± 0.01 m, while the final mass is 1.5 ± 0.4 kg ($D = 210 \pm 20$ kg m $^{-2}$). The relatively low ablated mass ratio of about 57 per cent is attributable to the very low pre-atmospheric speed of 12.8 ± 0.2 km s $^{-1}$ and also to the steep inclination of the trajectory. Compared to values given in Tab. 1, the pre-atmospheric mass for the Cavezzo meteorite is the lowest ever reported between ‘pedigree’ meteorites. From the pre-atmospheric mass and velocity estimates, the impact energy results to be 0.07 ± 0.02 T TNT, which is also the lowest among values given in Tab. 1.

3.3 Atmospheric data

The knowledge of the atmospheric conditions plays a key role in the computation of the dark flight and strewn-field of meteorite fragments to be found on ground. In particular, the wind direction and intensity are the major drivers for the loss of accuracy of these results. This effect is even more important in our case, given the small residual mass after ablation and the even smaller expected mass and size of the fragments (order of 100 g / 1 cm). For these reasons, we specifically computed the atmospheric state for the Cavezzo area at the time of fall.

Meteorological data came from IOIS (Integrated Observations Ingesting System) elaborated and used at Meteo Expert, a private organisation providing meteorological services where weather models are internally developed and applied. All available data, coming from surface, upper air and remote sensing measurements, are integrated to produce initialisation to be perturbed for a limited-area ensemble prediction system. A variational quality control is applied to check data consistency (Steinacker et al. 2011; Tavolato & Isaksen 2015); the observation is compared with the background and surrounding observations to determine its analysis weight in the system. This procedure is applied to develop perturbed initial data for usual forecast

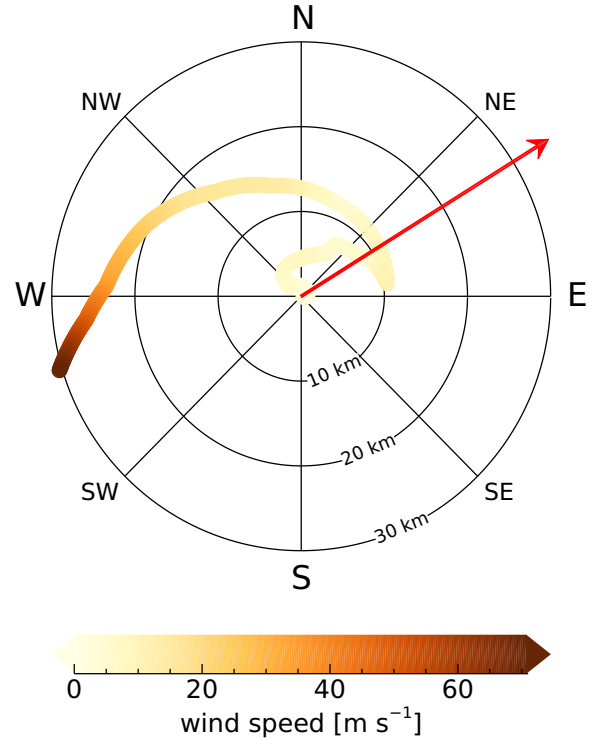


Figure 5. Wind vertical profile at 18 UTC in the Cavezzo area used for the strewn-field computation. The red arrow shows the fireball motion direction on ground.

model, that runs at 00, 06, 12 and 18 UTC. However, in our case as for several other applications including nowcasting, an hourly 3D grid is needed. This grid follows the model’s horizontal mesh size at 3.5 km, while in the vertical fifty variable-depth levels are used from surface to stratosphere. The scaling of weather parameters at a defined location is made interpolating values by surrounding grid points, with a correction algorithm which takes into account sub-grid terrain characteristics and local gradients.

3.4 Dark flight and strewn-field

Figure 5 shows the wind intensity and direction values at 18 UTC in the Cavezzo area, as a function of the altitude. The wind was particularly intense at about 22 km, which is the last observed point of the luminous path, reaching about 28 m s $^{-1}$ and blowing at 45° clockwise with respect to the meteoroid motion direction. The wind intensity decreases to reach about 20 m s $^{-1}$ at 20 km altitude and is confined below 10 m s $^{-1}$ from 13 km downwards. This led to a significant shift of the strewn-field compared to a situation with zero wind, especially in the transverse direction.

Figure 6 shows the computed strewn-field for the Cavezzo meteorite, together with the terminal part of the luminous atmospheric trajectory projected on ground (red line), and the location where the two fragments were recovered (purple star). By assuming that a fragmentation occurred, the impact point computed with a purely ablative model is not representative of the real case. Therefore, we computed the expected impact point for fragments with different mass-section ratio, ranging from $D = 30$ up to 200 kg m $^{-2}$, which is approximately the final value for the main-mass pure ablation (Sect.

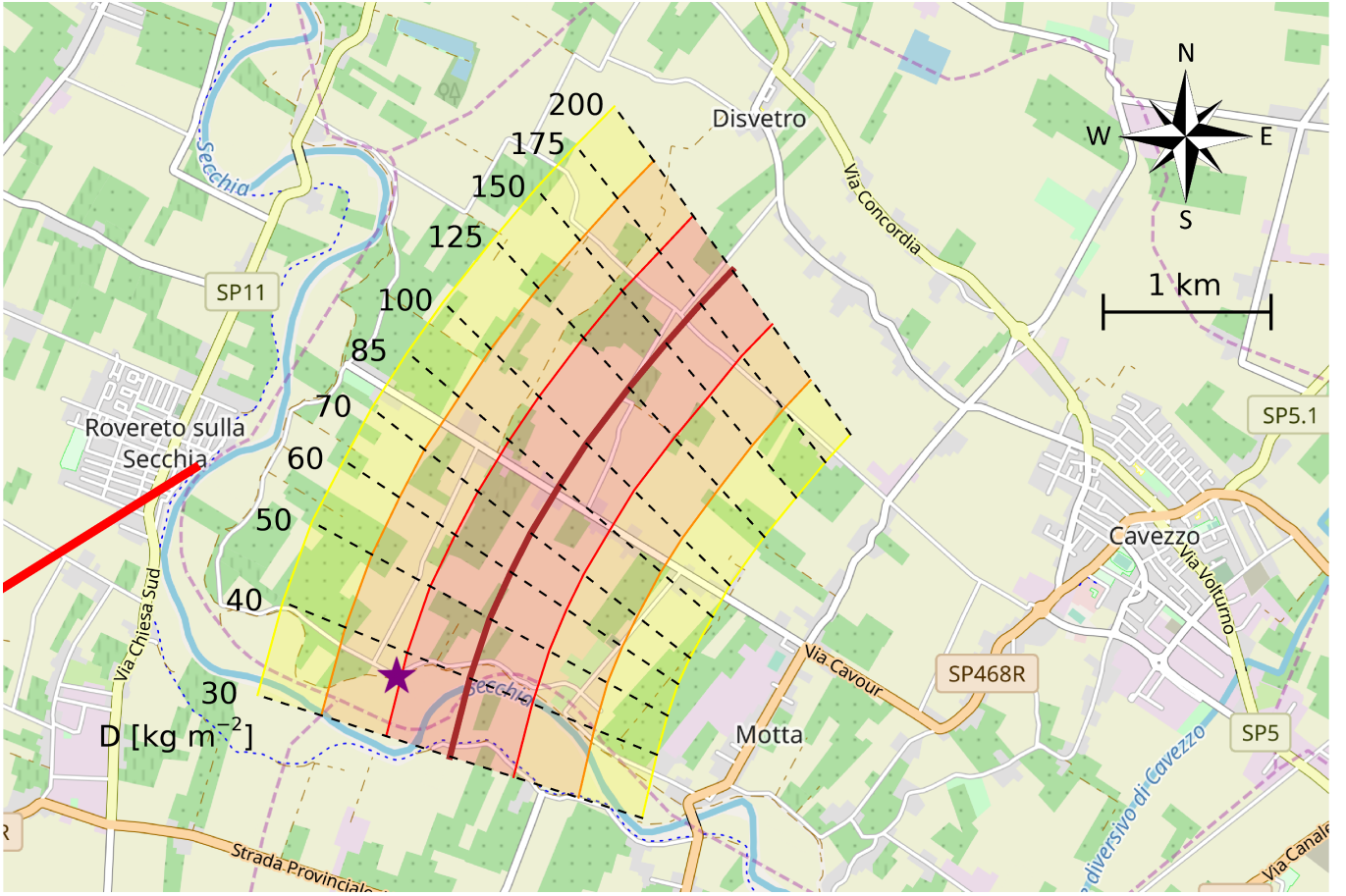


Figure 6. Strewn-field for the Cavezzo meteorite fragments, as a function of different mass-section ratio values (dashed black lines) from 30 up to 200 kg m^{-2} . The brown thick line shows the nominal impact point and the shaded areas enclose 1σ (red), 2σ (orange) and 3σ (yellow) uncertainties in the transverse direction. The purple star shows where the two Cavezzo fragments F1 and F2 were recovered, and the thick red line plots the terminal part of the bright flight trajectory, projected on ground. Background map data copyrighted OpenStreetMap contributors and available from <https://www.openstreetmap.org>.

Table 4. Data regarding the nominal impact points with different D final values. From top to bottom: final mass-section value, latitude and longitude of the impact point, shift parallel (L) and orthogonal (X) to motion direction of the bright flight and on-ground impact velocity.

Quantity											
Final D [kg m^{-2}]	30	40	50	60	70	85	100	125	150	175	200
Lat. N impact point [$^{\circ}$]	44.8245	44.8287	44.8318	44.8343	44.8364	44.8390	44.8412	44.8441	44.8466	44.8486	44.8504
Long. E impact point [$^{\circ}$]	10.9759	10.9773	10.9789	10.9804	10.9819	10.9841	10.9862	10.9893	10.9921	10.9947	10.9971
L [km, ± 0.3]	0.4	0.7	1.0	1.2	1.5	1.8	2.0	2.4	2.7	3.0	3.3
X [km, ± 0.4]	2.3	1.9	1.7	1.5	1.4	1.2	1.1	1.0	0.8	0.8	0.7
v_{impact} [m s^{-1}]	28	32	36	39	42	47	51	56	62	66	71

3.4). The brown thick line shows the most probable impact point as a function of D , while the red/orange/yellow shaded areas represent the $1/2/3\sigma$ uncertainty, respectively, in the transverse direction. The 1σ uncertainty in the longitudinal direction can be estimated to be 300 m. Table 4 reports the impact parameters for the sampled D values. The lateral displacement (X) can be as high as 2.3 km for smaller fragments. The expected impact velocity ranges from 28 to 71 m s^{-1} . The position of the recovered fragments lies at the very border of the 1σ transverse interval, in a region where recovered fragments are expected to have mass-section ratio values between 30 and 50 kg m^{-2} . The D values for the two fragments can be estimated

to be 30 – 70 kg m^{-2} for F1 and 35 – 85 kg m^{-2} for F2, considering that we ignore the meteorites orientation during the fall. Therefore, the mass-section ratio for both F1 and F2 is compatible with the predicted values of the dark-flight model. However, since the meteorite very likely fragmented on ground due to the impact, the D value of the original body remains unknown.

Table 5. Orbital elements of the Cavezzo meteoroid (left) and of 2013 VC₁₀ from NEODyS (right).

Quantity	Cavezzo	2013 VC ₁₀
Semi major axis [AU]	1.82 ± 0.22	1.56622
Eccentricity	0.460 ± 0.063	0.365295
Inclination [°]	4.0 ± 1.6	2.044
Long. of ascending node [°]	280.52311 ± 0.00001	224.068
Argument of Perihelion [°]	179.2 ± 4.8	240.264
Longitude of Perihelion [°]	99.7 ± 4.8	104.332
Perihelion passage [JD]	2458849.6 ± 0.5	2458808.1
Perihelion distance [AU]	0.983 ± 0.001	0.9941
Aphelion distance [AU]	2.66 ± 0.41	2.1383
<i>U</i>	0.216 ± 0.001	0.1818
<i>θ</i> [°]	22.96 ± 0.30	24.8358
<i>φ</i> [°]	175.90 ± 0.69	171.49
<i>λ</i> _⊕ [°]	100.52311 ± 0.00001	104.986

4 A POSSIBLE PROGENITOR OF THE CAVEZZO METEORITE

Using the value of $12.8 \pm 0.2 \text{ km s}^{-1}$ for the pre-atmospheric velocity, we computed the heliocentric orbit of the meteoroid prior to the impact. The true geocentric speed results to be $5.8 \pm 0.5 \text{ km s}^{-1}$. The orbital elements are reported in Tab. 5. The apparent radiant ($\alpha_a = 6^\circ 5 \pm 0^\circ 2$, $\delta_a = 30^\circ 6 \pm 0^\circ 2$) is located in the Andromeda constellation, while the true radiant ($\alpha_t = 358^\circ 4 \pm 0^\circ 3$, $\delta_t = 24^\circ 4 \pm 0^\circ 3$) is in Pegasus. The computed heliocentric orbit, shown as the red ellipse (nominal value) and shaded area (1σ uncertainty) in Fig. 7, has moderate eccentricity and low inclination on the Ecliptic, with a Tisserand invariant with respect to Jupiter equal to 4.1 ± 0.2 , thus indicating that the progenitor meteoroid was of asteroidal origin.

To find possible progenitor(s) of the Cavezzo meteorite, we follow the procedure described in Carbognani et al. (2020), using the orbital similarity criterion D_N introduced by Valsecchi et al. (1999); the NEODyS database⁸ conveniently lists the secular quantities used in D_N for all Near-Earth Asteroids (NEAs) for which they are defined. We use D_N in the form:

$$D_N = \sqrt{(U - U_c)^2 + (\cos \theta - \cos \theta_c)^2 + \Delta \xi^2}, \quad (2)$$

with:

$$\Delta \xi^2 = \min \left[\Delta \phi_I^2 + \Delta \lambda_I^2, \Delta \phi_{II}^2 + \Delta \lambda_{II}^2 \right]$$

$$\begin{cases} \Delta \phi_I = 2 \sin \frac{\phi - \phi_c}{2} \\ \Delta \phi_{II} = 2 \sin \frac{180^\circ + \phi - \phi_c}{2} \\ \Delta \lambda_I = 2 \sin \frac{\lambda_\oplus - \lambda_{\oplus,c}}{2} \\ \Delta \lambda_{II} = 2 \sin \frac{180^\circ + \lambda_\oplus - \lambda_{\oplus,c}}{2} \end{cases}.$$

In the above expressions, U , θ , ϕ , λ_\oplus refer to the NEA, and are taken from NEODyS, while U_c , θ_c , ϕ_c , $\lambda_{\oplus,c}$ are those of the Cavezzo meteorite (Tab. 5). Details on the definition of the variables and on D_N are given in Valsecchi et al. (1999). We looked for NEAs for which $D_N \leq 0.15$. The search resulted in only one candidate, 2013 VC₁₀, for which proper elements are given in the last column of Tab. 5;

⁸ NEODyS-2 database – <https://newton.spacedys.com/~neodyS2/propneo/encounter.cond>

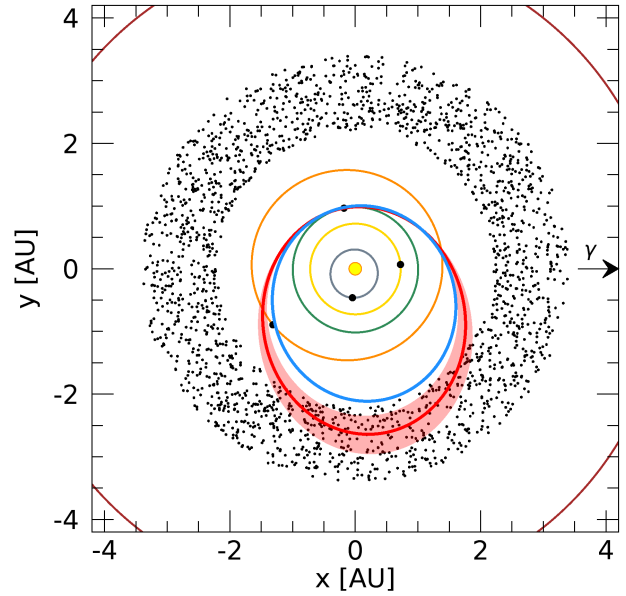


Figure 7. The reconstructed heliocentric orbit for the progenitor meteoroid of the Cavezzo meteorite (red ellipse) as seen from the ecliptic north pole and projected onto the ecliptic plane, together with the 1σ uncertainty band (shaded red area). The blue ellipse plots the 2013 VC₁₀ orbit (for which orbital elements are provided by the NEODyS database). Remaining ellipses plot Solar System planets' orbits up to Jupiter, and the black dots indicates their position along the orbit at the time of the IT20200101 fireball. The black small dots symbolically represent the asteroid Main Belt.

for the pair Cavezzo-2013 VC₁₀, $D_N = 0.115$. The nominal orbit of 2013 VC₁₀, projected onto the ecliptic plane, is shown in Fig. 7 (blue ellipse). There is a reasonable similarity between the two orbits, that is more evident if one considers the secular quantities that enter the computation of D_N . On the other hand, the pair Cavezzo-2013 VC₁₀ is rather isolated in the 4-dimensional space U , θ , ϕ , λ_\oplus ; this isolation is recognisable even in the 2-dimensional space constituted by the ecliptical radiant coordinates. Figure 8 shows the radiants of the pair Cavezzo-2013 VC₁₀, as well as the radiants of the simulated impactors of Chesley & Spahr (2004), and of the 20 real impactors listed in Granvik & Brown (2018). As discussed in the Appendix of Farnocchia et al. (2012), the radiant distribution simply reflects the distribution of the values of the semi-major axis, eccentricity and inclination of those NEAs whose orbits actually can cross that of the Earth; as a result, NEA impactor radiants are not uniformly distributed in a plot like Fig. 8a, but presents concentrations and regions of low density that are even more evident in Fig. 8b. It is in one of the low-density regions that the pair Cavezzo-2013 VC₁₀ is located, lending some additional credibility to the possible association.

5 CONCLUSIONS

After less than three years of operations, the PRISMA network, partner of FRIPON, has achieved one of its major objectives, i.e. the recovery of the first Italian meteorite by computation of a precise strewn-field through the analysis of its observational data. Two meteorite fragments, fallen near Cavezzo (Modena) on New Year's day 2020, weighing 3.6 and 51.7 grams, were recovered three days

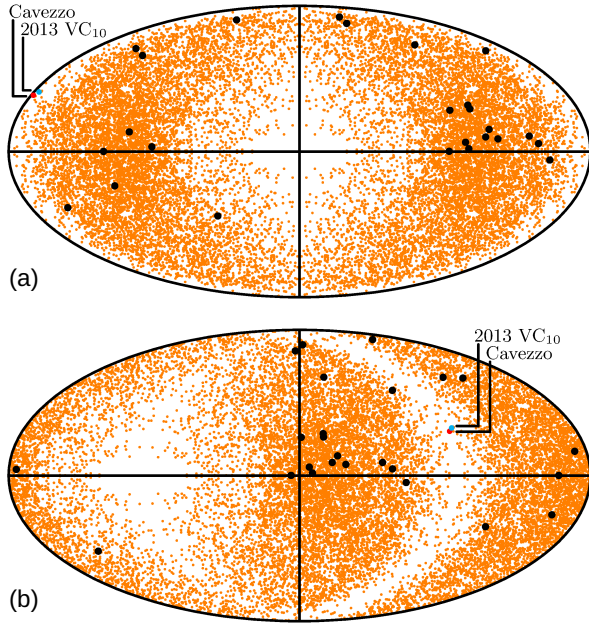


Figure 8. The radiant of the Cavezzo meteoroid (red dot) and of 2013 VC₁₀ (cyan dot) in an equal area projection of the sky centred on the apex of the Earth motion (a) and on the opposition (b); the angular coordinates are ecliptic longitude minus the longitude of the Sun, and ecliptic latitude. The orange dots are the radiant of the simulated impactors of Chesley & Spahr (2004), while the black dots are the radiant of the 20 meteorites listed in Granvik & Brown (2018).

after the fall as a result of a dedicated field search and thanks to the involvement of the local people, at a distance of 400 m from the nominal computed position, very close to the 1σ uncertainty position. They were immediately recognised as freshly fallen meteorites, a fact that has been confirmed by the unquestionable presence of short-lived cosmogenic radio-isotopes (such as ^{48}V , half-life of 15.97 d) measured with a very sensitive γ -ray detector at the Monte dei Cappuccini Laboratory in Torino. The analyses, carried out at the Department of Earth Sciences of the Firenze University (Pratesi et al. 2020, submitted), highlighted strong differences between the two specimens and therefore a proposal has been submitted to the Nomenclature Committee of the Meteoritical Society in order to require a classification as anomalous L-chondrite.

The computed orbital parameters and the value of the Tisserand invariant ($T_J = 4.1 \pm 0.2$) indicate an asteroidal origin of the meteoroid, located in the inner part of the main belt. The proper elements, compared with the ones of known NEAs from the NEODyS database, show that among those only one asteroid, namely 2013 VC₁₀, is compatible with the Cavezzo meteoroid. Moreover, the radiant of both objects are located in a low-density region of NEA impactors, thus lending additional credibility to the association.

The associated fireball trajectory, seen by many eyewitnesses, was characterised by an entry velocity of $12.2 \pm 0.2 \text{ km s}^{-1}$ and by a high inclination angle of $68.4 \pm 0.3^\circ$. The luminous path started at a height of $75.9 \pm 0.2 \text{ km}$ and reached $21.5 \pm 0.1 \text{ km}$, after travelling approximately 59 km in 5.6 s. The absolute magnitude reached a minimum of -9.5 at 32.6 km of altitude, where a bright flash was seen, very likely indicating a fragmentation and followed by a second flash reaching -8.5 , while in the brightest part of the trajectory the mean absolute magnitude was around -7.5 . By assuming a purely ablative regime,

spherical form of the meteoroid and given the measured meteorite bulk density of 3.322 g cm^{-3} , the estimated residual mass is $1.5 \pm 0.4 \text{ kg}$.

The pre-atmospheric mass and velocity of $3.5 \pm 0.8 \text{ kg}$ and $12.8 \pm 0.2 \text{ km s}^{-1}$ respectively, leading to a total impact energy of less than 0.07 T TNT, together with the brightest absolute magnitude reached, are the lowest among the ones estimated for the 35 meteorites with pedigree recovered so far, listed in Tab. 1. This recovery can therefore be considered up to now the most challenging in terms of size and magnitude of the associated event, and proves the adequacy of the network and of our reduction pipeline also in such demanding conditions.



ACKNOWLEDGEMENTS

PRISMA is the Italian Network for Systematic surveillance of Meteors and Atmosphere. It is a collaboration initiated and coordinated by the Italian National Institute for Astrophysics (INAF) that counts members among research institutes, universities, associations and schools. The complete list of PRISMA members is available here: <http://www.prisma.inaf.it>. PRISMA was partially funded by 2016/0476 and 2019/0672 *Research and Education* grants from Fondazione Cassa di Risparmio di Torino and by a 2016 grant from Fondazione Agostino De Mari (Savona). PRISMA data are hosted and made available to the public by the INAF research e-infrastructure project IA2 (Italian Center for Astronomical Archives).

FRIPON was funded by the ANR grant N.13-BS05-0009-03, carried by the Paris Observatory, Muséum National d'Histoire Naturelle, Paris-Saclay University and Institut Pythéas (LAM-CEREGE). FRIPON data are hosted and processed at Institut Pythéas SIP (Service Informatique Pythéas), and a mirror is hosted at IMCCE (Institut de Mécanique Céleste et de Calcul des Éphémérides / Paris Observatory) with the help of IDOC (Integrated Data and Operation Center), supported by CNRS and CNES.

The PRISMA collaboration is grateful to Mr. Davide Gaddi, who recovered the meteorite fragments, allowed for the analysis of the samples and eventually decided to donate them to INAF.

Background map data for Fig. 6 copyrighted OpenStreetMap contributors and available from <https://www.openstreetmap.org>, distributed under the Open Data Commons Open Database License (<https://opendatacommons.org/licenses/odbl/>)

REFERENCES

- Audureau Y., et al., 2014, in Proceedings of the 33th International Meteor Conference, Giron, France, 18 - 21 September 2014, pp 39–41
- Barghini D., Gardiol D., Carbognani A., 2019a, in Proceedings of the 37th International Meteor Conference Pezinok-Modra, Slovakia, 30 August - 2 September 2018, pp 41–45
- Barghini D., Gardiol D., Carbognani A., Mancuso S., 2019b, *A&A*, **626**, A105
- Bischoff A., et al., 2011, *Meteorit. Planet. Sci.*, **46**, 793
- Bischoff A., Dyl K. A., Horstmann M., Ziegler K., Wimmer K., Young E. D., 2013, *Meteorit. Planet. Sci.*, **48**, 628
- Bischoff A., et al., 2017, *Meteorit. Planet. Sci.*, **52**, 1683
- Bischoff A., et al., 2019, *Geochemistry / Chem. Erde*, **79**, 125525
- Bland P. A., et al., 2009, *Science*, **325**, 1525
- Bland P. A., et al., 2016, in 79th Annual Meeting of the Meteoritical Society, p. 6265
- Borovička J., 1990, *Bull. Astron. Inst. Czechoslov.*, **41**, 391
- Borovička J., Kalenda P., 2003, *Meteorit. Planet. Sci.*, **38**, 1023
- Borovička J., Spurný P., Kecklikova J., 1995, *A&AS*, **112**, 173

- Borovička J., Popova O. P., Nemtchinov I. V., Spurný P., Ceplecha Z., 1998, *A&A*, **334**, 1713
- Borovička J., Spurný P., Kalenda P., Tagliaferri E., 2003a, *Meteorit. Planet. Sci.*, **38**, 975
- Borovička J., et al., 2003b, *Meteorit. Planet. Sci.*, **38**, 1005
- Borovička J., Charvát Z., 2009, *A&A*, **507**, 1015
- Borovička J., et al., 2013a, *Meteorit. Planet. Sci.*, **48**, 1757
- Borovička J., Spurný P., Brown P., Wiegert P., Kalenda P., Clark D., Shrubený L., 2013b, *Nature*, **503**, 235
- Borovička J., et al., 2015, *Meteorit. Planet. Sci.*, **50**, 1244
- Borovička J., Popova O., Spurný P., 2019, *Meteorit. Planet. Sci.*, **54**, 1024
- Bouvier A., Gattacceca J., Agee C., Grossman J., Metzler K., 2017, *Meteorit. Planet. Sci.*, **52**, 2284
- Brown P., Ceplecha Z., Hawkes R. L., Wetherill G., Beech M., Mossman K., 1994, *Nature*, **367**, 624
- Brown P. G., et al., 2000, *Science*, **290**, 320
- Brown P. G., Revelle D. O., Tagliaferri E., Hildebrand A. R., 2002, *Meteorit. Planet. Sci.*, **37**, 661
- Brown P., Pack D., Edwards W. N., Revelle D. O., Yoo B. B., Spalding R. E., Tagliaferri E., 2004, *Meteorit. Planet. Sci.*, **39**, 1781
- Brown P., et al., 2011, *Meteorit. Planet. Sci.*, **46**, 339
- Brown P. G., et al., 2013, *Nature*, **503**, 238
- Brown P. G., et al., 2019, *Meteorit. Planet. Sci.*, **54**, 2027
- Carbognani A., et al., 2020, *Eur. Phys. J. Plus*, **135**, 255
- Ceplecha Z., 1961, *Bull. Astron. Inst. Czechoslov.*, **12**, 21
- Ceplecha Z., 1987, *Bull. Astron. Inst. Czechoslov.*, **38**, 222
- Ceplecha Z., 1996, *A&A*, **311**, 329
- Ceplecha Z., Revelle D. O., 2005, *Meteorit. Planet. Sci.*, **40**, 35
- Chesley S. R., Spahr T. B., 2004, in *Mitigation of Hazardous Comets and Asteroids*. p. 22
- Clark D. L., Wiegert P. A., 2011, *Meteorit. Planet. Sci.*, **46**, 1217
- Colas F., et al., 2014, in *Proceedings of the 33th International Meteor Conference*, Giron, France, 18-21 September 2014. pp 18–21
- Colas F., et al., 2015, in *Proceedings of the 34th International Meteor Conference*, Mistelbach, Austria, 27-30 August 2015. pp 37–40
- Colombetti P., Taricco C., Bhandari N., Sinha N., Di Martino M., Cora A., Vivaldo G., 2013, *Nucl. Instrum. Methods Phys. Res. A*, **718**, 140
- Devillepoix H. A. R., et al., 2018, *Meteorit. Planet. Sci.*, **53**, 2212
- Devillepoix H. A. R., et al., 2019, *MNRAS*, **483**, 5166
- Dyl K. A., et al., 2016, *Meteorit. Planet. Sci.*, **51**, 596
- Farnocchia D., Bernardi F., Valsecchi G. B., 2012, *Icarus*, **219**, 41
- Ferus M., et al., 2020, *Icarus*, **341**, 113670
- Foschini L., 1999, *A&A*, **342**, L1
- Gardiol D., Cellino A., Di Martino M., 2016, in *Proceedings of the 35th International Meteor Conference* Egmond, the Netherlands, 2-5 June 2016. pp 76–79
- Gardiol D., et al., 2019, in *Proceedings of the 37th International Meteor Conference* Pezinok-Modra, Slovakia, 30 August - 2 September 2018. pp 81–86
- Gattacceca J., Bouvier A., Grossman J., Metzler K., Uehara M., 2019, *Meteorit. Planet. Sci.*, **54**, 469
- Gattacceca J., McCubbin F. M., Bouvier A., Grossman J., 2020, *Meteorit. Planet. Sci.*, **55**, 460
- Gounelle M., Spurný P., Bland P. A., 2006, *Meteorit. Planet. Sci.*, **41**, 135
- Granvik M., Brown P., 2018, *Icarus*, **311**, 271
- Haack H., et al., 2012, *Meteorit. Planet. Sci.*, **47**, 30
- Haack H., et al., 2019, *Meteorit. Planet. Sci.*, **54**, 1853
- Halliday I., Griffin A. A., Blackwell A. T., 1981, *Meteoritics*, **16**, 153
- Hildebrand A. R., McCausland P. J. A., Brown P. G., Longstaffe F. J., Russell S. D. J., Tagliaferri E., Wacker J. F., Mazur M. J., 2006, *Meteorit. Planet. Sci.*, **41**, 407
- Hildebrand A. R., et al., 2009, in *Lunar and Planetary Science Conference*. Lunar and Planetary Science Conference. p. 2505
- Hunter J. D., 2007, *Comput. Sci. Eng.*, **9**, 90
- Jenniskens P., et al., 2009, *Nature*, **458**, 485
- Jenniskens P., et al., 2012, *Science*, **338**, 1583
- Jenniskens P., et al., 2014, *Meteorit. Planet. Sci.*, **49**, 1388
- Jenniskens P., et al., 2019, *Meteorit. Planet. Sci.*, **54**, 699
- Jenniskens P., et al., 2020, *Meteorit. Planet. Sci.*, **55**, 535
- Kalenichenko V. V., 2006, *A&A*, **448**, 1185
- Knapic C., De Marco M., Smareglia R., Molinaro M., 2014, in *Astronomical Data Analysis Software and Systems XXIII*. p. 131
- Kohout T. J., et al., 2017, *Meteorit. Planet. Sci.*, **52**, 1525
- Kruijer T. S., Kleine T., Borg L. E., 2020, *Nat. Astron.*, **4**, 32
- Llorca J., et al., 2005, *Meteorit. Planet. Sci.*, **40**, 795
- McCrosky R. E., Posen A., Schwartz G., Shao C. Y., 1971, *J. Geophys. Res.*, **76**, 4090
- Milley E. P., Hildebrand A. R., Brown P. G., Noble M., Sarty G., Ling A., Maillet L. A., 2010, in *GeoCanada 2010*.
- Palotai C., Sankar R., Free D. L., Howell J. A., Botella E., Batcheldor D., 2019, *MNRAS*, **487**, 2307
- Popova O., Borovička J., Hartmann W. K., Spurný P., Gnos E., Nemtchinov I., Trigo-Rodríguez J. M., 2011, *Meteorit. Planet. Sci.*, **46**, 1525
- Popova O. P., et al., 2013, *Science*, **342**, 1069
- Pratesi G., et al., 2020, *Meteorit. Planet. Sci.* (submitted)
- Revelle D. O., Brown P. G., Spurný P., 2004, *Meteorit. and Planet. Sci.*, **39**, 1605
- Sansom E. K., et al., 2020, arXiv e-prints, p. arXiv:2006.07151
- Shaddad M. H., et al., 2010, *Meteorit. Planet. Sci.*, **45**, 1557
- Simon S. B., Grossman L., Clayton R. N., Mayeda T. K., Schwade J. R., Sipiera P. P., Wacker J. F., Wadhwa M., 2004, *Meteorit. Planet. Sci.*, **39**, 625
- Spurný P., 1994, *Planet. Space Sci.*, **42**, 157
- Spurný P., Heinlein D., Oberst J., 2002, in *Warmbein B., ed., ESA Special Publication Vol. 500, Asteroids, Comets, and Meteors: ACM 2002*. pp 137–140
- Spurný P., Oberst J., Heinlein D., 2003, *Nature*, **423**, 151
- Spurný P., Borovička J., Kac J., Kalenda P., Atanackov J., Kladnik G., Heinlein D., Grau T., 2010, *Meteorit. Planet. Sci.*, **45**, 1392
- Spurný P., Bland P. A., Shrubený L., Towner M. C., Borovička J., Bevan A. W. R., Vaughan D., 2011, *Meteorit. Planet. Sci. Suppl.*, **74**, 5101
- Spurný P., et al., 2012, *Meteorit. Planet. Sci.*, **47**, 163
- Spurný P., Haloda J., Borovička J., Shrubený L., Halodová P., 2014, *A&A*, **570**, A39
- Spurný P., Borovička J., Haloda J., Shrubený L., Heinlein D., 2016, in *79th Annual Meeting of the Meteoritical Society*. p. 6221
- Spurný P., Borovička J., Baumgarten G., Haack H., Heinlein D., Sørensen A. N., 2017a, *Planet. Space Sci.*, **143**, 192
- Spurný P., Borovička J., Mücke H., Svoreň J., 2017b, *A&A*, **605**, A68
- Spurný P., Bland P. A., Borovička J., Towner M. C., Shrubený L., Bevan A. W. R., Vaughan D., 2019, in *Meteoroids 2019, Bratislava, Slovakia, 17-21 June 2019*. p. 6369
- Spurný P., Borovička J., Shrubený L. J., 2020, *Meteorit. Planet. Sci.*, **55**, 376
- Steinacker R., Mayer D., Steiner A., 2011, *Mon. Weather Rev.*, **139**, 3974
- Taricco C., Bhandari N., Cane D., Colombetti P., Verma N., 2006, *J. Geophys. Res.*, **111**, A08102
- Tavolato C., Isaksen L., 2015, *Q. J. R. Meteorol. Soc.*, **141**, 1514
- Tóth J., et al., 2015, *Meteorit. Planet. Sci.*, **50**, 853
- Trigo-Rodríguez J. M., Borovička J., Spurný P., Ortiz J. L., Docobo J. A., Castro-Tirado A. J., Llorca J., 2006, *Meteorit. Planet. Sci.*, **41**, 505
- Trigo-Rodríguez J. M., et al., 2015, *MNRAS*, **449**, 2119
- Unsalan O., et al., 2019, *Meteorit. Planet. Sci.*, **54**, 953
- Valsecchi G. B., Jopek T. J., Froeschle C., 1999, *MNRAS*, **304**, 743
- Welten K. C., Meier M. M. M., Caffee M. W., Nishiizumi K., Wieler R., Jenniskens P., Shaddad M. H., 2010, *Meteorit. Planet. Sci.*, **45**, 1728
- Wilson G., McCausland P., 2012, *Can. J. Earth Sci.*, **50**, 4

AFFILIATIONS

¹*INAF - Osservatorio Astrofisico di Torino, Via Osservatorio 20, 10025 Pino Torinese, TO, Italy*

²*Università degli Studi di Torino - Dipartimento di Fisica, via Pietro Giuria 1, 10153 Torino, TO, Italy*

³*INAF - Osservatorio di Astrofisica e Scienza dello Spazio, Via*

Piero Gobetti 93/3, 40129 Bologna, BO, Italy

⁴INAF - Osservatorio Astronomico d'Abruzzo, Via Mentore Maggini SNC, Località Collurania, 64100 Teramo, TE, Italy

⁵INAF - Osservatorio Astronomico di Trieste, Via Giambattista Tiepolo 11, 10134 Trieste, TS, Italy

⁶Università degli Studi di Firenze - Dipartimento di Scienze della Terra, Via Giorgio La Pira, 4, 50121 Firenze, FI, Italy

⁷INAF - Istituto di Astrofisica e Planetologia Spaziali, Via del Fosso del Cavaliere 100, 00133 Roma, RM, Italy

⁸Osservatorio Astronomico del Righi, Via Mura delle Chiappe 44R, 16136 Genova, GE, Italy

⁹Meteo Expert, Via Giovanni Frova, 34, 20092 Cinisello Balsamo, MI, Italy

¹⁰IFAC - CNR, Via Madonna del Piano 10, 50019 Sesto Fiorentino, FI, Italy

¹¹IMCCE, Observatoire de Paris, PSL Research University, CNRS UMR 8028, Sorbonne Université, Université de Lille, 77 av. Denfert-Rochereau, 75014 Paris, France

¹²FRIPON (Fireball Recovery and InterPlanetary Observation) and Vigie-Ciel Team, France

¹³Institut de Minéralogie, Physique des Matériaux et Cosmochimie (IMPMC), Muséum National d'Histoire Naturelle, CNRS UMR 7590, Sorbonne Université, 75005 Paris, France

¹⁴GEOPS - Géosciences, CNRS, Université Paris-Saclay, 91405 Orsay, France

¹⁵Service Informatique Pythéas (SIP) CNRS - OSU Institut Pythéas - UMS 3470, Marseille, France

¹⁶Aix Marseille Université, CNRS, IRD, Coll France, INRA, CEREGE, Aix-en-Provence, France

¹⁷International Meteor Organization

¹⁸Aix Marseille Université, CNRS, CNES, LAM, Marseille, France

¹⁹La Torre del Sole, Via Caduti sul Lavoro 2, 24030 Brembate di Sopra, BG, Italy

²⁰Associazione Astrofilo Bisalta, Via Gino Eula 23, 12013 Chiusa di Pesio, CN, Italy

²¹Associazione Sky Sentinel, Via Giovanni Leone 36, 81020 San Nicola la Strada, CE, Italy

²²Meteoriti Italia APS, Via Fusina 6, 32032 Feltre, BL, Italy

²³GAMP - Osservatorio Astronomico Montagna Pistoiese, 51028 San Marcello Piteglio, PT, Italy

²⁴Gruppo Astrofilo Antares, Via Garibaldi 12, 48033 Cotignola, RA, Italy

²⁵INAF - Osservatorio Astronomico di Brera, Via Brera 28, 20121 Milano, MI, Italy

²⁶Associazione Astronomica del Rubicone, Via Palmiro Togliatti 5, 47039 Savignano sul Rubicone, FC, Italy

²⁷INAF - Osservatorio Astrofisico di Catania, Via Santa Sofia 78, 95123 Catania, CT, Italy

²⁸SpaceDyS, Via Mario Giuntini 63, 56023 Navacchio di Cascina, PI, Italy

²⁹Università di Firenze - Osservatorio Polifunzionale del Chianti, Strada Provinciale Castellina in Chianti, 50021 Barberino Val D'Elsa, FI, Italy

³⁰Associazione Astrofilo Urania, Località Bric del Colletto 1, 10062 Luserna San Giovanni, TO, Italy

³¹INAF - Osservatorio Astronomico di Capodimonte, Salita Moiarriello 16, 80131 Napoli, NA, Italy

³²Associazione Astrofilo Tethys - Planetario e Osservatorio Astronomico di Ca' del Monte, Località Ca' del Monte, 27050 Cecima, PV, Italy

³³Associazione Culturale Googol, Via Filippo Brunelleschi 21, 43100 Parma, PR, Italy

³⁴INAF - Osservatorio Astronomico di Padova, Vicolo dell'Osservatorio 5, 35122 Padova, PD, Italy

³⁵Fondazione GAL Hassin - Centro Internazionale per le Scienze Astronomiche, Via della Fontana Mitri, 90010 Isnello, PA, Italy

³⁶Planetarium Pythagoras, Via Margherita Hack, 89125 Reggio Calabria, RC, Italy

³⁷Università del Salento - Dipartimento di Matematica e Fisica, Via Per Arnesano, 73100 Lecce, LE, Italy

³⁸Liceo Statale 'Arturo Issel', Via Fiume 42, 17024 Finale Ligure, SV, Italy

³⁹Gruppo Astrofilo Monti Lepini - Osservatorio Astronomico e Planetario di Gorga, 00030 Gorga, RM, Italy

⁴⁰Università di Camerino - Scuola di Scienze e Tecnologie, sezione Geologia, via Gentile III da Varano, 62032 Camerino, MC, Italy

⁴¹Gruppo Astrofilo Montelupo Fiorentino, Piazza Vittorio Veneto 10, 50056 Montelupo Fiorentino, FI, Italy

⁴²Università di Padova - Dipartimento di Fisica e Astronomia, Vicolo dell'Osservatorio 3, 35122 Padova, PD, Italy

⁴³Osservatorio Astrofisico R.P. Feynman, 73034 Gagliano del Capo, LE, Italy

⁴⁴Osservatorio Astronomico di Sormano, Località Colma di, 22030 Sormano, CO, Italy

⁴⁵INAF - Osservatorio Astrofisico di Arcetri, Largo Enrico Fermi 5, 50125 Firenze, FI, Italy

⁴⁶Associazione Astrofilo di Piombino - Osservatorio Astronomico Punta Falcone, Punta Falcone, Località Falcone, 57025 Piombino, LI, Italy

⁴⁷INAF - Osservatorio Astronomico di Cagliari, Via della Scienza 5, 09047 Cuccuru Angius, Selargius, CA, Italy

⁴⁸INAF - Istituto di Radioastronomia, Via Piero Gobetti 101, 40129 Bologna, BO, Italy

⁴⁹CIRA - Centro Italiano Ricerche Aerospaziali, Via Maiorise snc, 81043 Capua, CE, Italy

⁵⁰Astrobioparco Oasi di Felizzano, Strada Fubine 79, 15023 Felizzano, AL, Italy

⁵¹Università degli Studi di Firenze - Dipartimento di Fisica e Astronomia, Via Sansone 1, 50019 Sesto Fiorentino, FI, Italy

⁵²IIS 'E.Fermi' di Montesarchio, Via Vitulanese, 82016 Montesarchio, BN, Italy

⁵³Liceo Scientifico Statale 'G.B. Quadri', Viale Giosuè Carducci 17, 36100 Vicenza, VI, Italy

⁵⁴Università degli Studi di Trento - Dipartimento di Ingegneria Civile, Ambientale e Meccanica, Via Mesiano 77, 38123 Trento, TN, Italy

⁵⁵Osservatorio Astronomico Sirio, Piazzale Anelli, 70013 Castellana Grotte, BA, Italy

⁵⁶Museo del Cielo e della Terra, Vicolo Baciadonne 1, 40017 San Giovanni in Persiceto, BO, Italy

⁵⁷Università del Piemonte Orientale - Dipartimento di Scienze e Innovazione Tecnologica, Viale Teresa Michelin 11, 15121 Alessandria, AL, Italy

⁵⁸Osservatorio Astronomico Giuseppe Piazzi, Località San Bernardo, 23026 Ponte in Valtellina, SO, Italy

⁵⁹Liceo Scientifico Statale 'P. Paleocapa', Via Alcide De Gasperi 19, 45100 Rovigo, RO, Italy

⁶⁰Osservatorio Astronomico Bobhouse, Via Giuseppe Tomasi P. pe di Lampedusa 9, 90147 Palermo, PA, Italy

This paper has been typeset from a $\text{\TeX}/\text{\LaTeX}$ file prepared by the author.